Geophysical Research Letters

Does ocean coupling matter for the northern extratropical response to projected Arctic sea ice loss?

Clara Deser[1], Lantao Sun[2], Robert A. Tomas[1], and James Screen[3]

[1]Climate and Global Dynamics Division, National Center for Atmospheric Research, Boulder, Colorado, USA, [2]Cooperative Institute for Research in Environmental Sciences, University of Colorado Boulder and NOAA Earth System Research Laboratory, Boulder, Colorado, USA, [3]College of Engineering, Mathematics and Physical Sciences, University of Exeter, Exeter, UK

Abstract The question of whether ocean coupling matters for the extratropical Northern Hemisphere atmospheric response to projected late 21st century Arctic sea ice loss is addressed using a series of experiments with Community Climate System Model version 4 at 1° spatial resolution under different configurations of the ocean model component: no interactive ocean, thermodynamic slab ocean, and full-depth (dynamic plus thermodynamic) ocean. Ocean-atmosphere coupling magnifies the response to Arctic sea ice loss but does not change its overall structure; however, a slab ocean is inadequate for inferring the role of oceanic feedbacks. The westerly winds along the poleward flank of the eddy-driven jet weaken in response to Arctic sea ice loss, accompanied by a smaller-magnitude strengthening on the equatorward side, with largest amplitudes in winter. Dynamical and thermodynamic oceanic feedbacks amplify this response by approximately 50%. Air temperature, precipitation, and sea level pressure responses also show sensitivity to the degree of ocean coupling.

1. Introduction

The continued loss of Arctic sea ice is one of the most anticipated consequences of global warming, with projections for a seasonally ice-free Arctic Ocean by 2100 if current rates of greenhouse gas (GHG) emissions continue unabated [*Intergovernmental Panel on Climate Change*, 2013]. The melting of Arctic sea ice is expected to have important consequences for atmospheric circulation and climate at middle and high latitudes due to the altered surface energy balance of the Arctic Ocean as highly reflective ice cover is replaced by darker open water [e.g., *Serreze and Barry*, 2011]. Without the insulating layer of sea ice, newly exposed (and relatively warm) surface waters flux heat and water vapor into the overlying atmosphere, warming and moistening the lower troposphere [e.g., *Screen and Simmonds*, 2010]. High-frequency atmospheric motions transport this excess heat and moisture over the adjacent northern continents, leading to increases in air temperature and precipitation [*Deser et al.*, 2010; *Screen et al.*, 2015b]. In addition to local thermodynamic effects, diminished Arctic sea ice cover weakens the tropospheric westerly winds along the poleward flank of the jet stream, especially in winter. The weakened westerlies occur in association with a reduced north-south temperature gradient due to enhanced warming of the Arctic lower troposphere [*Deser et al.*, 2010; *Peings and Magnusdottir*, 2014; *Deser et al.*, 2015; *Harvey et al.*, 2013, 2015; *Sun et al.*, 2015]. Influences of Arctic sea ice loss on the north-south meandering of the jet stream and associated synoptic activity including blocking events are less certain [*Barnes*, 2013; *Screen and Simmonds*, 2013; *Cohen et al.*, 2014; *Barnes and Screen*, 2015; *Hassanzadeh and Kuang*, 2015; *Francis and Vavrus*, 2015]. In some regions, for example, central Eurasia, Arctic sea ice loss may paradoxically lead to surface cooling as a result of an enhanced Siberian anticyclone and associated cold-air advection [*Honda et al.*, 2009; *Mori et al.*, 2014; *Sun et al.*, 2015; *Kug et al.*, 2015], although this dynamical cooling is not expected to outweigh warming due to other atmospheric circulation changes in the future [*Mori et al.*, 2014].

While most of the climate impacts from Arctic sea ice loss occur at middle and high latitudes of the Northern Hemisphere (NH), recent work demonstrates that ocean-atmosphere coupling may extend their reach into the tropics and Southern Hemisphere [*Deser et al.*, 2015, hereafter D15]. In that study, dynamical ocean processes were shown to play a central role in communicating the effects of Arctic sea ice loss to lower latitudes. In addition to expanding the geographical influence of Arctic sea ice loss, air-sea interaction also modifies the local (extratropical NH) zonal mean temperature and zonal wind responses to Arctic sea ice loss (D15).

The purpose of this study is to provide a more comprehensive analysis of the effects of air-sea coupling on the extratropical NH atmospheric circulation and surface climate response to projected Arctic sea ice loss using a hierarchy of climate model simulations in which oceanic feedbacks are either suppressed entirely, limited to thermodynamic processes, or represented in full (e.g., including dynamical mechanisms). Unlike D15 who focused on only two models in this hierarchy, we systematically compare all three configurations. In addition, we analyze the spatial patterns of response in atmospheric circulation, temperature, precipitation, and sea surface temperature (SST), going beyond the zonal mean view presented in D15. Changes in ocean circulation and heat transport in the fully coupled experiment are presented in D15.

The remainder of this study is organized as follows. The models and experimental design are provided in section 2. Results are presented in section 3. Key findings are discussed and summarized in section 4.

2. Models and Experimental Design

We make use of existing simulations presented in D15, along with two new experiments, to reveal the effects of air-sea coupling in the atmospheric response to projected late 21st century Arctic sea ice loss. All experiments use the Community Climate System Model version 4 (CCSM4) at 1° spatial resolution, configured with different versions of the ocean component: (1) no (interactive) ocean model (NOM: SSTs and sea ice are prescribed), (2) slab (thermodynamic mixed layer) ocean model (SOM), and (3) full-depth (dynamic plus thermodynamic) ocean model (FOM). Details of the model configurations, experimental design, and Arctic sea ice loss may be found in D15; only a brief synopsis is given below. CCSM4 realistically simulates the climatological distribution of Arctic sea ice concentration and thickness, as well as its interannual variability and trends over the past few decades [*Kay et al.*, 2011; *Jahn et al.*, 2012; *Wettstein and Deser*, 2014]. Other aspects of the model's climatology and variability are presented in the CCSM4 Special Issue Collection of the *Journal of Climate* (2012).

To artificially control Arctic sea ice in the SOM and FOM, D15 introduced an additional seasonally varying longwave radiative flux (LRF) to the sea ice model at each Arctic grid box to achieve a desired seasonal cycle of sea ice concentration and thickness under present-day GHG conditions (see Appendix in D15 for details of the LRF). Two such experiments were conducted: one that targets sea ice conditions at the end of the twentieth century (the 1980–1999 average from six CCSM4 historical simulations), and one that targets conditions at the end of the 21st century (the 2080–2099 average from six CCSM4 Representative Concentration Pathway 8.5 (RCP8.5) simulations). These simulations are termed SOM_20 and SOM_21 (FOM_20 and FOM_21) based on the SOM (FOM) model configurations with late 20th and 21st centuries sea ice conditions, respectively (Table S1 in the supporting information). Differencing the 20th and 21st century SOM (FOM) simulations isolates the impact of projected Arctic sea ice loss on the thermodynamically coupled (fully coupled) climate system, since both are run under present-day (year 2000) GHG concentrations.

We emphasize that (1) all of the prescribed LRF goes directly into the sea ice model component (e.g., the LRF is a "ghost flux" to both the atmosphere and ocean model components); (2) there is no conduction of heat between the sea ice and ocean model components; and (3) the amount of LRF specified to the ice model at a particular grid box at any given time is proportional to the ice fraction in the grid box at that time. Thus, the prescribed LRF does not directly affect the climate system: it impacts the ocean and atmosphere only via the changes it induces in Arctic sea ice.

A climatological spatially varying monthly "Qflux" derived from FOM_20 is specified to both SOM_20 and SOM_21 to represent the mean effects of present-day ocean heat transport on SST; in addition, climatological spatially varying annual mean mixed layer depths (MLDs) from FOM_20 are specified to both SOM_20 and SOM_21.

Two new simulations are conducted here using the NOM version of the model in which sea ice concentration and thickness as well as SSTs are specified to the atmospheric model. For the NOM_20 experiment, the *global* sea ice and SST conditions from FOM_20 are specified; for the NOM_21 experiment, the *Arctic* sea ice and SST conditions from FOM_21 are specified, with sea ice and SST conditions over the rest of the globe taken from FOM_20 (Table S1). The difference between the two NOM experiments isolates the effect of 21st century Arctic sea ice loss on the atmosphere-land system in the absence of ocean feedbacks (GHG levels were fixed at the year 2000 in both NOM simulations). (Note that the equivalent NOM experiments

presented in D15 were based on sea ice and SST conditions from the CCSM4 historical and RCP8.5 simulations, which are slightly different from those in the FOM_20 and FOM_21 experiments used here.)

The SOM and FOM experiments were run for 300 and 360 years, respectively, and the last 260 years are used for analysis following D15. The NOM experiments were run for 260 years, and all years are used for analysis. In the following, we refer to the difference between the 260 year averages from NOM_21 and NOM_20 as ΔICE_NOM, and similarly for the SOM and FOM experiments. The statistical significance of all responses is assessed using a two-sided Student's t test applied to the difference between the two 260 year averages and their corresponding standard deviations.

The seasonal cycles of the change in Arctic sea ice area between the late 20th and late 21st centuries are nearly identical across the three experiments (ΔICE_NOM, ΔICE_SOM, and ΔICE_FOM), with the greatest losses in late summer and autumn (maximum amplitude $\sim 7 \times 10^6$ km^2 in October) and the smallest reductions in late winter (minimum amplitude $\sim 2 \times 10^6$ km^2 in March; Figure S1a). This means that we can attribute any differences in their atmospheric responses mainly to the effects of ocean coupling. Spatially, sea ice loss in autumn (September–November) is largely confined to the central Arctic basin, whereas in winter, it occurs mainly in the peripheral seas (Sea of Okhotsk, Bering and Beaufort Seas in the Pacific, and Labrador, Greenland and Barents Seas and Hudson Bay in the Atlantic: Figure S1b).
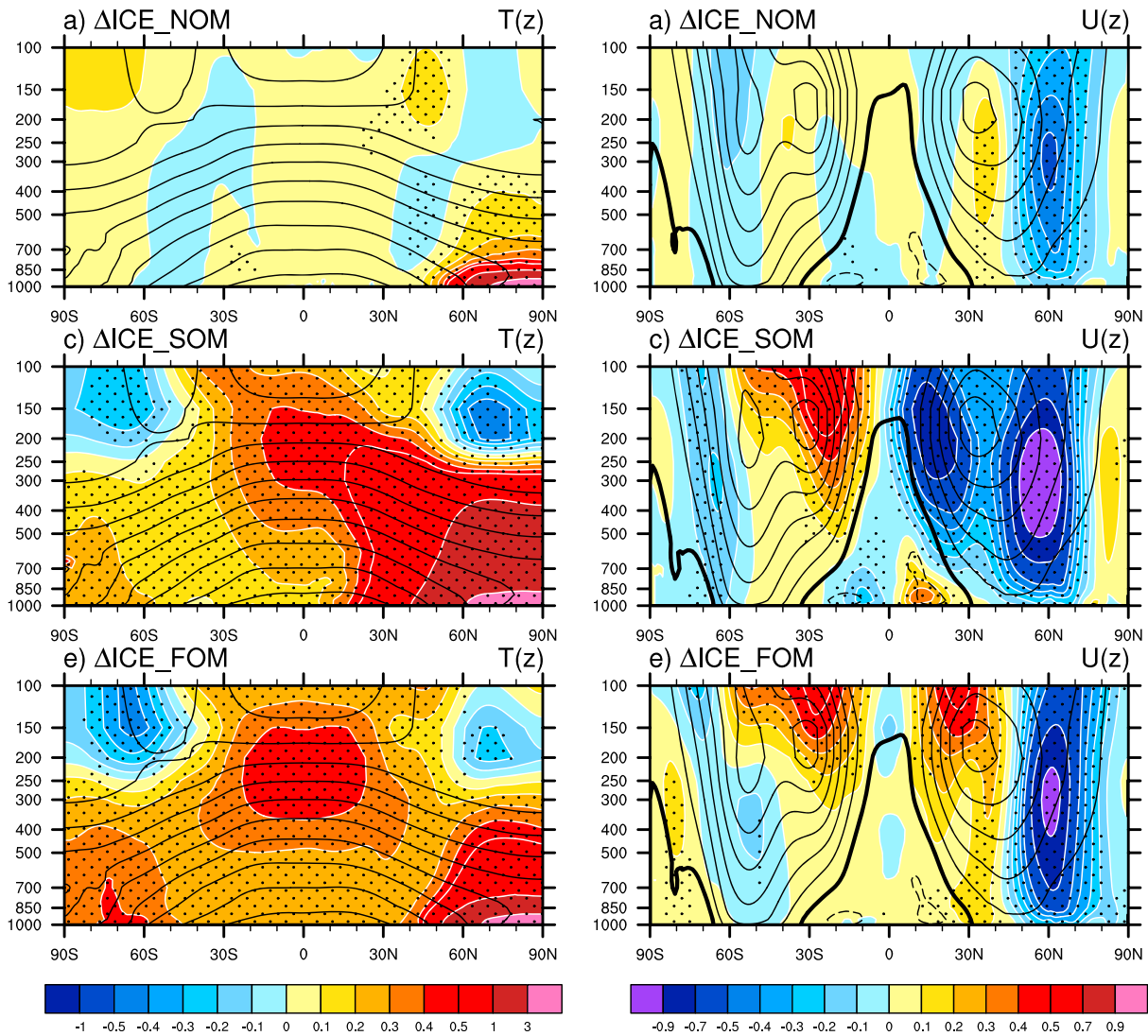
The reduction in sea ice cover results in an anomalous net upward surface energy flux (Q_{net}) from the Arctic Ocean to the atmosphere, with the maximum Q_{net} response (70 W m^{-2} in November–January) lagging the peak sea ice loss by 2–3 months in all three experiments (Figure S1a). This delay is due to the effect of the seasonal cycle of the climatological air-sea temperature difference on the turbulent energy flux response as discussed in *Deser et al.* [2010]. There are some small (5–10 W m^{-2}) differences in the magnitude of the wintertime Q_{net} response among the experiments, due to slight differences in the amount of sea ice loss and surface temperature of the ice (not shown). However, the overall similarity of the sea ice loss and Q_{net} responses in the three experiments allows us to deduce the effects of dynamical and thermodynamic oceanic feedbacks on the atmospheric response to projected Arctic sea ice loss.

3. Results

3.1. Global Zonal Mean Response to Arctic Sea Ice Loss

We begin with a global view of the annual zonal mean atmospheric temperature and zonal wind responses to Arctic sea ice loss in the three ocean model configurations (Figure 1). Significant responses in ΔICE_NOM are confined to the northern extratropics, with surface-intensified warming north of 50°N (maximum values > 8°C at 1000 hPa in the Arctic) and weakened (strengthened) westerlies on the poleward (equatorward) flank of the eddy-driven jet (maximum amplitudes approximately 0.5 m s^{-1} at 60°N and 0.2 m s^{-1} at 35°N in the upper troposphere near 250–300 hPa). Compared to the uncoupled experiment, the coupled experiments show stronger high-latitude warming in the free troposphere, with values of approximately 0.15°C in ΔICE_NOM, 1.40°C in ΔICE_SOM, 0.60°C in ΔICE_FOM at 500 hPa. The amplified polar warming in the free troposphere in the coupled experiments leads to a larger-amplitude zonal wind response, with maximum values at 60°N and 300 hPa of 1.0 m s^{-1} in ΔICE_FOM and 1.2 m s^{-1} in ΔICE_SOM, compared to 0.5 m s^{-1} in ΔICE_NOM. A notable difference between the westerly wind responses in ΔICE_SOM and ΔICE_FOM is their latitudinal extent: ΔICE_SOM shows a broader band (40°–70°N) of reduced westerlies compared to ΔICE_FOM (50°–70°N). In addition, ΔICE_SOM shows no significant zonal wind change on the equatorward side of the eddy-driven jet (although the equatorward side of the thermally driven subtropical jet weakens in the latitude band 10°–25°N), unlike ΔICE_FOM which shows a strengthening of the westerlies in the region 30°–40°N. In summary, ΔICE_FOM shows a similar pattern of response in the northern extratropics as ΔICE_NOM but with approximately twice the amplitude; and both exhibit structural differences with the response in ΔICE_SOM.

In addition to local effects, ocean coupling extends the atmospheric response to Arctic sea ice loss into the tropics and Southern Hemisphere (SH). However, the latitudinal structures of the global-scale responses differ markedly between ΔICE_FOM and ΔICE_SOM. In particular, ΔICE_SOM shows a strong interhemispheric gradient in tropospheric warming magnitude, whereas ΔICE_FOM shows a more equatorially symmetric structure. These distinctive thermal patterns are associated with different zonal mean zonal wind changes. In particular, the cross-equatorial temperature gradient in ΔICE_SOM results in opposite-signed zonal wind

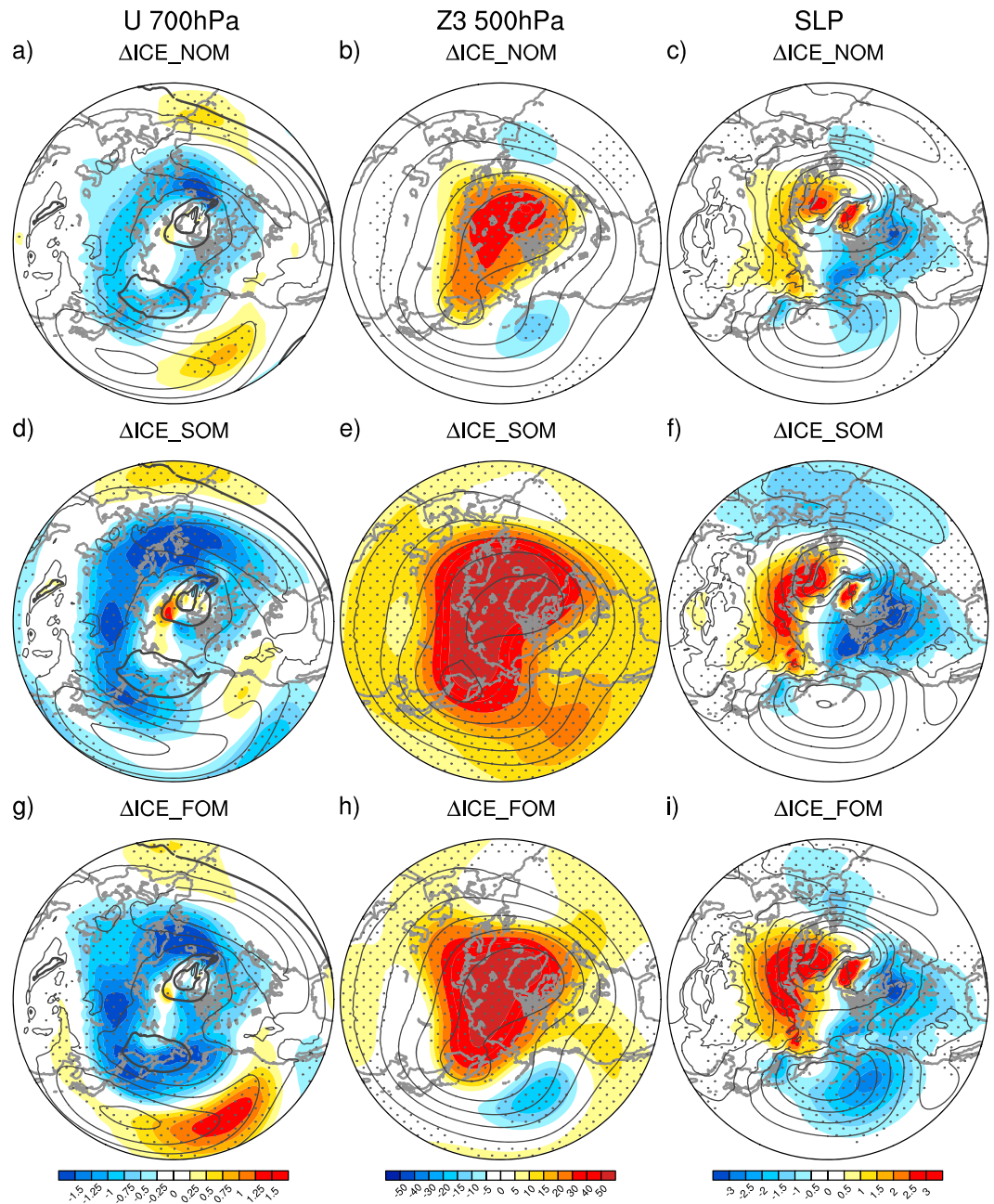**Figure 1.** Annual zonal mean (a, c, e) temperature (°C) and (b, d, f) zonal wind (m s^{-1}) responses to Arctic sea ice loss in the in ΔICE_NOM (Figures 1a and 1b), ΔICE_SOM (Figures 1c and 1d), and ΔICE_FOM (Figures 1e and 1f) model configurations (color shading: color bars at the bottom of each column; note the nonlinear color scales). Stippling indicates where the response is statistically significant at the 95% confidence level. Contours indicate the twentieth century climatology (contour interval of 10°C for temperature and 5 m s^{-1} for zonal wind with the zero contour thickened).

anomalies on the equatorward flanks of the thermally driven subtropical jet of the two hemispheres, whereas the equatorially symmetric tropical warming in ΔICE_FOM is associated with like-signed subtropical zonal wind changes. In addition, ΔICE_SOM shows a small but statistically significant weakening of the westerlies on the poleward flank of the eddy-driven jet in the SH, whereas ΔICE_FOM shows a weak positive zonal wind response near Antarctica. Both coupled experiments feature enhanced warming at upper levels in the tropics, as well as some amplification of the lower tropospheric warming at high southern latitudes.

The response of the NH westerlies to Arctic sea ice loss exhibits a pronounced seasonal cycle, with largest amplitudes during boreal winter (Figure S2) when the net upward surface energy flux response over the Arctic Ocean is greatest (recall Figure S1a). The zonal mean temperature and zonal wind responses in the tropics and NH in December-January-February (DJF) are similar to those in the annual mean, but their magnitudes are approximately twice as large (Figure S3). The SH responses in DJF are generally insignificant except in ΔICE_FOM, which shows a small but statistically significant weakening of the westerlies on the poleward flank of the eddy-driven jet near 50°–60°S, analogous to that in the NH (Figure S3).

Figure 2. DJF 700 hPa zonal wind (U700; m s^{-1}), 500 hPa geopotential height (Z500; m), and SLP (hPa) responses to Arctic sea ice loss in the (a–c) ΔICE_NOM, (d–f) ΔICE_SOM, and (g–i) ΔICE_FOM model configurations. Stippling indicates where the response is statistically significant at the 95% confidence level. Contours indicate the twentieth century climatology (contour interval of 5 m s^{-1} for U700 with the zero contour thickened, 500 m for Z500 and 10 hPa for SLP).

3.2. Spatial Patterns of Response to Arctic Sea Ice Loss

For the remainder of this study, we focus on the wintertime (DJF) extratropical NH atmospheric response to projected Arctic sea ice loss. Spatial patterns of the DJF 700 hPa zonal wind (U700), 500 hPa geopotential height (Z500), and sea level presssure (SLP) responses are shown in Figure 2 (annual means are shown in Figure S4). The weakening of the lower tropospheric zonal winds at high latitudes is apparent over all longitudes in all three model configurations; however, the midlatitude strengthening of the westerlies occurs preferentially in the Pacific and east Atlantic sectors. The positive U700 anomalies in the east Atlantic/west African sector are indicative of a strengthening of the equatorward flank of the eddy-driven jet, but in the
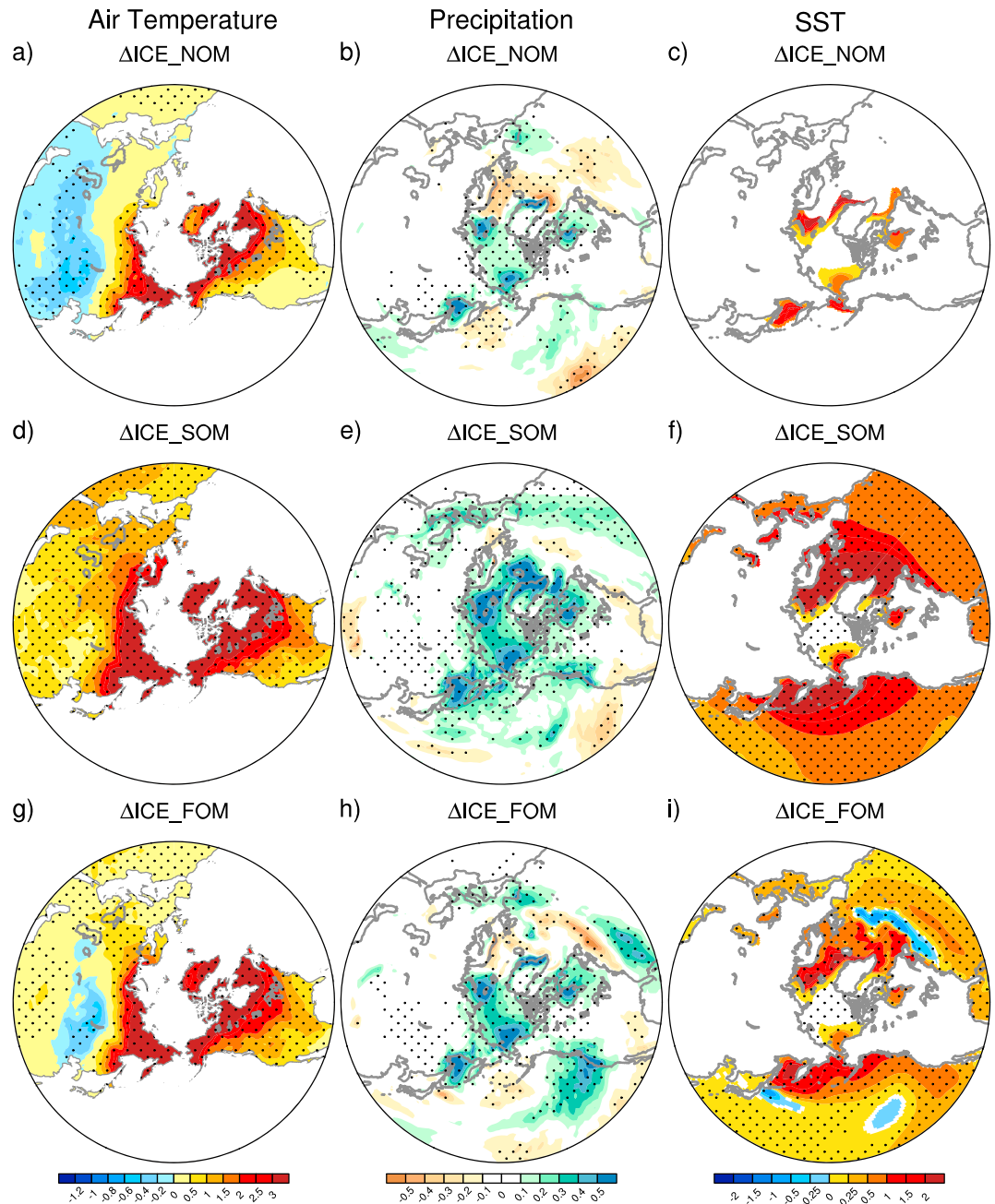
Pacific sector they represent a downstream strengthening of the jet core. Thus, caution is needed when relating climatology and response based on zonal averages. Overall, the U700 response patterns are very similar between ΔICE_NOM and ΔICE_FOM, with differences primarily in magnitude, consistent with the zonal mean results. ΔICE_SOM, however, shows some notable differences: in particular, the high-latitude band of easterly wind anomalies in the Atlantic extends farther south into the main core of the jet, and the midlatitude band of westerly wind anomalies in the Pacific is virtually absent.

The Z500 response in ΔICE_NOM projects onto the negative polarity of the Northern Annular Mode (NAM), with positive values in the polar region and negative values farther south in the eastern Atlantic and Pacific (Figure 2). The elevated Z500 values over the polar cap are a direct consequence of the warming of the lower troposphere in response to Arctic sea ice loss, as found in many previous studies [e.g., *Deser et al.*, 2010; *Screen et al.*, 2015a]. The polar Z500 response is amplified in both coupled experiments, consistent with the greater warming of the free troposphere. The negative NAM response pattern is still discernible in ΔICE_FOM, although it is embedded within a positive background Z500 response. In contrast, ΔICE_SOM is dominated by a general increase in Z500.

The SLP response in each of the experiments exhibits a continental wave-one pattern, with positive values over northern Eurasia and negative values over Canada (Figure 2). The magnitude of the SLP response over Eurasia is largest in ΔICE_FOM and smallest in ΔICE_NOM (maximum values ~ 4.0 hPa and 2.7 hPa, respectively), while the response over Canada is greatest in ΔICE_SOM (maximum values ~ 4 hPa compared to ~ 3 hPa in the other experiments). In addition to this continental dipole pattern, negative SLP anomalies occur over the eastern Atlantic and Pacific, with larger magnitudes in ΔICE_FOM compared to ΔICE_NOM. ΔICE_SOM lacks the deepened Aleutian Low and overestimates the negative SLP response over the eastern Atlantic and Mediterranean compared to ΔICE_FOM and ΔICE_NOM. These differences can be traced to differences in their tropical precipitation responses (not shown). The dynamical mechanisms that give rise to the distinctive continental wave-one SLP pattern remain to be elucidated. Previous atmosphere-only studies indicate that the high-pressure response over Eurasia is related to sea ice loss in the Barents-Kara Sea region [e.g., *Mori et al.*, 2014; *Kug et al.*, 2015]. Further work is needed to assess the impact of sea ice loss in other areas.

The DJF 2 m air temperature, precipitation, and SST responses to Arctic sea ice loss are shown in Figure 3 (recall that ΔICE_NOM has prescribed SST anomalies in regions of sea ice loss, taken from ΔICE_FOM). All three experiments show warming over the high-latitude continents, with maximum values exceeding 5°C near the Arctic border. This terrestrial warming is primarily confined to the highest latitudes in ΔICE_NOM, whereas it extends over the entire North American continent in both coupled experiments, and over all of Eurasia in ΔICE_SOM. A swath of cooling extends across Eurasia from the Ural Mountains to the Pacific Ocean in ΔICE_NOM. This decrease in air temperature is dynamically induced by the positive SLP response over Siberia, which brings anomalously cold northeasterly flow to the region. Note that the magnitude of the cooling is modest (generally < 0.5°C). There is no trace of negative temperature anomalies in ΔICE_SOM, and only a vestige of cooling in ΔICE_FOM, despite that the positive SLP response over Siberia is stronger in both coupled experiments compared to ΔICE_NOM. It is likely that the continent-wide warming in ΔICE_SOM is due to thermodynamic effects associated with increased SSTs, which outweigh the dynamically induced cooling associated with the Siberian high-pressure response. Similarly, the weak residual cooling in ΔICE_FOM likely reflects a combination of stronger dynamically induced cooling and smaller thermodynamically induced warming due to smaller SST increases compared to ΔICE_SOM.

The patterns of precipitation response are largely similar in all experiments, with regional differences in magnitude. Within the Arctic, the largest precipitation increases occur directly over regions of sea ice loss, with magnitudes in excess of 0.5 mm d^{-1} in ΔICE_NOM and more than 0.6 mm d^{-1} in ΔICE_SOM and ΔICE_FOM. Both ΔICE_NOM and ΔICE_FOM exhibit decreased precipitation over the far northern Atlantic and Pacific, likely in association with the negative net surface heat flux response in these regions (not shown, but see *Deser et al.* [2010]). ΔICE_FOM shows a distinctive north-south dipole pattern of precipitation response over the North Atlantic that coincides with underlying changes in SSTs (increased precipitation associated with warmer SSTs and vice versa). The distinctive pattern of SST response in ΔICE_FOM is associated with a southward shift of the Gulf Stream and its extension. This dynamically induced SST response is necessarily lacking in ΔICE_SOM, which shows instead a relatively bland pattern of oceanic warming that increases monotonically northward in both basins. A significant increase in precipitation occurs over the eastern North Pacific and western United States in ΔICE_FOM, likely driven by the deepened Aleutian Low;

Figure 3. DJF surface air temperature (°C; land only), precipitation (mm d^{-1}), and SST (°C) responses to Arctic sea ice loss in the (a–c) ΔICE_NOM, (d–f) ΔICE_SOM, and (g–i) ΔICE_FOM model configurations. Stippling indicates where the response is statistically significant at the 95% confidence level. White shading in Figures 3c, 3f, and 3i denotes absolute values < 0.01°C.

this feature is also present to some extent in both ΔICE_NOM and ΔICE_SOM but with weaker amplitude and fewer areas of statistical significance.

4. Discussion and Conclusions

We have examined the NH extratropical atmospheric response to projected Arctic sea ice loss using a hierarchy of model configurations in which oceanic feedbacks are either suppressed entirely, limited to thermodynamic processes, or represented in full. We find that ocean-atmosphere coupling amplifies the atmospheric circulation response to Arctic sea ice loss by approximately 50% but does not change its overall structure; however, both

dynamical and thermodynamic processes must be included for a proper representation of oceanic feedbacks. As in many other studies, we find that Arctic sea ice loss weakens the tropospheric westerlies along the poleward flank (50°–70°N) of the eddy-driven jet, accompanied by a smaller-magnitude increase to the south (30°–40°N). This response is strongest in winter, despite that the sea ice loss is largest in autumn. The weakening of the westerly winds on the poleward side of the jet occurs at all longitudes, whereas the increase to the south occurs preferentially over the eastern ocean basins and shows a different relationship to the climatological winds in the Atlantic and Pacific. The reduction in high-latitude westerlies is consistent with thermal wind balance in response to warming of the Arctic lower troposphere. The SLP response shows a distinctive continental wave-one pattern, with positive anomalies over northern Eurasia and negative anomalies over northern North America. The dynamical mechanisms that give rise to this pattern remain to be elucidated, in particular, the contributions from sea ice loss in different regions.

Air-sea coupling also enhances the magnitude of the near-surface air temperature and precipitation responses to projected Arctic sea ice loss, in particular, warming over the northern continents and precipitation increases over the central Arctic and the eastern North Pacific extending into western North America. These climate impacts are driven by a combination of thermodynamic and dynamical (circulation) effects. Although the dynamically induced cooling over central Eurasia is stronger with ocean feedbacks owing to the larger SLP response, it is outweighed by an even greater increase in thermodynamically induced warming resulting from elevated SSTs: the net effect of ocean coupling is thus to reduce the magnitude of near-surface cooling in central Eurasia. The southward shift of the Gulf Stream in response to Arctic sea ice loss produces a distinctive dipole pattern of SST anomalies in the North Atlantic that in turn drives a local precipitation dipole response: these features are unique to the fully coupled model.

The general amplifying effect of oceanic feedbacks on the atmospheric response to Arctic sea ice loss can be traced to an overall warming of the surface global oceans, which in turn warms and moistens the global troposphere through a combination of local and remote processes as discussed in D15. In particular, the enhanced warming of the northern extratropical free troposphere in ΔICE_FOM compared to ΔICE_NOM is due to increased poleward energy transport associated with a warmer and moister tropical upper troposphere as shown in D15. As a result, the atmospheric circulation response in the NH extratropics intensifies, with subsequent effects on the dynamically induced portion of the near-surface air temperature and precipitation responses. The thermodynamic (radiative) contribution to these responses is also enhanced by virtue of a warmer, moister atmosphere.

One might expect that thermodynamic air-sea coupling (e.g., as represented by a "slab" ocean mixed layer) would adequately represent the effects of ocean feedbacks on the atmospheric and surface climate response to Arctic sea ice loss. However, our experiments indicate that the slab ocean overestimates the local thermodynamic impact of air-sea coupling and modifies the spatial structure of the response compared to the full-depth ocean. Both shortcomings can be traced to the slab ocean's SST response, which is larger than that in the full-depth ocean model and which has a stronger gradient between the equator and the North Pole. The enhanced and southward expanded meridional gradient in the SST response leads to an overestimate of the magnitude and latitudinal width of the zonal wind response in middle latitudes in the slab ocean compared to the full-ocean coupled model configuration. A caveat is that the use of annual mean MLDs in the SOM experiments (the default configuration in CCSM4) may overestimate the magnitude of the SST response; however, the large-scale meridional (equator-to-pole) structure of the SST response is likely to be robust. Additional experiments are needed to verify these speculations.

Our experiments address the coupled climate system's response to an *abrupt* loss of Arctic sea ice (e.g., the sea ice in FOM_21 was forced to melt within a year, not shown). The extratropical NH atmospheric circulation adjusts quickly (within a few years) to the sudden loss of sea ice, even in the FOM experiment (Figure S6). Thus, the responses shown here can be viewed as being in quasi-equilibrium with the more gradual pace of sea ice loss that occurs in the RCP8.5 simulation over the course of the 21st century (not shown, but see *Stroeve et al.* [2012]). A full exploration of the mechanisms, patterns, and time scales of transient adjustment of the global coupled climate system to an abrupt loss of Arctic sea ice is beyond the scope of this study but will be pursued in future work. Finally, it should be noted that our study examines only the sea ice loss induced portion of climate change associated with an increase in GHG, not the full response to GHG forcing (see D15 for additional discussion).

References

Barnes, E. A. (2013), Revisiting the evidence linking Arctic amplification to extreme weather in midlatitudes, *Geophys. Res. Lett.*, *40*, 4728–4733, doi:10.1002/grl.50880.

Barnes, E. A., and J. A. Screen (2015), The impact of Arctic warming on the midlatitude jet-stream: Can it? Has it? Will it?, *WIREs Clim. Change*, *6*, 277–286, doi:10.1002/wcc.337.

Cohen, J., et al. (2014), Recent Arctic amplification and extreme mid-latitude weather, *Nat. Geosci.*, *7*, 627–637, doi:10.1038/ngeo2234.

Deser, C., R. Tomas, M. Alexander, and D. Lawrence (2010), The seasonal atmospheric response to projected Arctic sea ice loss in the late twenty-first century, *J. Clim.*, *23*, 333–351, doi:10.1175/2009JCLI3053.

Deser, C., R. A. Tomas, and L. Sun (2015), The role of ocean-atmosphere coupling in the zonal-mean atmospheric response to Arctic sea ice loss, *J. Clim.*, *28*, 2168–2186, doi:10.1175/JCLI-D-14-00325.1.

Francis, J. A., and S. J. Vavrus (2015), Evidence for a wavier jet stream in response to rapid Arctic warming, *Environ. Res. Lett.*, *10*, doi:10.1088/1748-9326/10/1/014005.

Harvey, B. J., L. C. Shaffrey, and T. J. Woollings (2013), Equator-to-pole temperature differences and the extra-tropical storm track responses of the CMIP5 climate models, *Clim. Dyn.*, *43*, 1–12.

Harvey, B. J., L. C. Shaffrey, and T. J. Woollings (2015), Deconstructing the climate change response of the Northern Hemisphere wintertime storm tracks, *Clim. Dyn.*, doi:10.1007/s00382-015-2510-8.

Hassanzadeh, P., and Z. Kuang (2015), Blocking variability: Arctic amplification versus Arctic oscillation, *Geophys. Res. Lett.*, *42*, 8586–8595, doi:10.1002/2015GL065923.

Honda, M., J. Inoue, and S. Yamane (2009), Influence of low Arctic sea ice minima on anomalously cold Eurasian winters, *Geophys. Res. Lett.*, *36*, L08707, doi:10.1029/2008GL037079.

Intergovernmental Panel on Climate Change (2013), *Climate Change 2013: The Physical Science Basis. Contribution of Working Group I to the Fifth Assessment Report of the Intergovernmental Panel on Climate Change*, edited by T. F. Stocker et al., 1535 pp., Cambridge Univ. Press, Cambridge, U. K., and New York, doi:10.1017/CBO9781107415324.

Jahn, A., et al. (2012), Late-twentieth-century simulation of Arctic sea ice and ocean properties in the CCSM4, *J. Clim.*, *25*, 1431–1452, doi:10.1175/JCLI-D-11-00201.1.

Kay, J. E., M. M. Holland, and A. Jahn (2011), Inter-annual to multi-decadal Arctic sea ice extent trends in a warming world, *Geophys. Res. Lett.*, *38*, L15708, doi:10.1029/2011GL048008.

Kug, J.-S., et al. (2015), Two distinct influences of Arctic warming on cold winters over North America and East Asia, *Nat. Geosci.*, *8*, 759–762, doi:10.1038/ngeo2517.

Mori, M., M. Watanabe, H. Shiogama, J. Inoue, and M. Kimoto (2014), Robust Arctic sea-ice influence on the frequent Eurasian cold winters in past decades, *Nat. Geosci.*, *7*, 869–873, doi:10.1038/ngeo2277.

Peings, Y., and G. Magnusdottir (2014), Response of the wintertime Northern Hemisphere atmospheric circulation to current and projected Arctic sea ice decline: A numerical study with CAM5, *J. Clim.*, *27*, 244–264, doi:10.1175/JCLI-D-13-00272.1.

Screen, J. A., and I. Simmonds (2010), Increasing fall-winter energy loss from the Arctic Ocean and its role in Arctic temperature amplification, *Geophys. Res. Lett.*, *37*, L16797, doi:10.1029/2010GL044136.

Screen, J. A., and I. Simmonds (2013), Exploring links between Arctic amplification and mid-latitude weather, *Geophys. Res. Lett.*, *40*, 959–964, doi:10.1002/grl.50174.

Screen, J. A., C. Deser and L. Sun (2015a), Reduced risk of North American cold extremes due to continued sea ice loss, *Bull. Am. Meteorol. Soc.*, *96*, 1489–1503, doi:10.1175/BAMS-D-14-00185.1.

Screen, J. A., C. Deser, and L. Sun (2015b), Projected changes in regional climate extremes arising from Arctic sea ice loss, *Environ. Res. Lett.*, *10*, 084006, doi:10.1088/1748-9326/10/8/084006.

Serreze, M. C., and R. G. Barry (2011), Processes and impacts of Arctic amplification: A research synthesis, *Global Planet. Change*, *77*, 85–96, doi:10.1016/j.gloplacha.2011.03.004.

Stroeve, J. C., V. Kattsov, A. Barrett, M. Serreze, T. Pavlova, M. Holland, and W. N. Meier (2012), Trends in Arctic sea ice extent from CMIP5, CMIP3 and observations, *Geophys. Res. Lett.*, *39*, L16502, doi:10.1029/2012GL052676.

Sun, L., C. Deser, and R. A. Tomas (2015), Mechanisms of stratospheric and tropospheric circulation response to projected Arctic sea ice loss, *J. Clim.*, *28*, 7824–7845, doi:10.1175/JCLI-D-15-0169.1.

Wettstein, J. J., and C. Deser (2014), Internal variability in projections of twenty-first century Arctic sea ice loss: Role of the large-scale atmospheric circulation, *J. Clim.*, *27*, 527–550, doi:10.1175/JCLI-D-12-00839.1.